

# Two-sensor-based $H_\infty$ control for nanopositioning in probe storage

Angeliki Pantazi, Abu Sebastian, Haralambos Pozidis, Evangelos Eleftheriou  
IBM Zurich Research Laboratory  
8803 Rüschlikon, Switzerland

**Abstract**—The ultra-high storage density in probe-storage devices makes positioning a significant challenge. The probes have to be positioned over the storage medium with nanoscale accuracy. A feedback-control scheme based on a high-precision global-positioning sensor can provide the required accuracy. However, drift and low frequency noise affect the performance over long periods of operation. A novel control architecture based on the  $H_\infty$  control framework is presented which addresses this problem by using medium-derived positional information along with the global-positioning sensor. This controller has a multiple-input single-output (MISO) structure and uses the best measurement in different frequency regions. Experimental results on a probe-storage device prototype demonstrate the efficacy of this approach.

## I. INTRODUCTION

Probe-storage devices are considered as an alternative to conventional data storage. In [1], [2] an implementation of a probe-storage device is described that is based on a thermomechanical principle for storing/retrieving information written on thin polymer films. Digital information is stored by making indentations on the thin polymer film with the tips of atomic force microscope (AFM) cantilevers, which are a few nanometers in diameter. To increase the data rate, an array of probes is used, in which each probe performs read/write/erase operations over an individual storage field with an area of  $100 \mu\text{m} \times 100 \mu\text{m}$ .

The shape of a typical indentation resembles an almost conical structure with a diameter of approx. 15 to 30 nm. This implies that the probes have to be positioned with very high accuracy over the storage medium. A miniaturized scanner with  $x/y$  motion capabilities of about  $120 \mu\text{m}$  is employed to position the storage medium with respect to the probe array. A control architecture for the micro-electro-mechanical system (MEMS) scanner is presented in [3]. The  $x/y$  positional information was provided by thermal position sensors [4]. Using these sensors, a closed-loop positioning resolution of approx. 2 nm was demonstrated [5].

Even though the thermal sensors have satisfactory noise performance in the high-frequency region, they tend to have a significant low-frequency component owing to ambient temperature variations. Hence a feedback-control scheme relying on the thermal sensors alone is not suitable for long-term operation of the device.

Because of the availability of multiple probes, a few probes and their respective storage fields could be dedicated for the generation of some form of medium-derived positional error signal (PES) [2]. This medium-derived PES accurately captures deviations from the track centerline for each data track. However, it has a very limited range of approx. 50 nm. Hence, even though the medium-derived PES does not suffer from drift, a feedback-control scheme relying

on that alone may not be appropriate for the storage device because of its limited range.

This motivated the design of a control architecture that utilizes both the thermal-sensor signal and the medium-derived PES. The objective of the design concept presented here is to create a control structure that utilizes the best measurement in different frequency regions. With the a-priori knowledge that thermal sensors are less reliable at low frequencies, the positional information from the medium-derived PES is primarily utilized for control at low frequencies. In the same vein, the thermal position sensor signal with high fidelity at high frequencies and unlimited range is preferred over the PES signal at high frequencies.

The  $H_\infty$  control framework was found to be appropriate to address such a “frequency division control”. The controller has a MISO structure, and the performance requirements are translated to appropriate weighting functions. In this paper we describe the solution to this problem and present its experimental validation on a probe-based storage prototype system. Note that the problem formulation is more general and can be applied to any control problem involving two sensors that have different performance characteristics in different frequency regions.

## II. SYSTEM DESCRIPTION

### A. Microscanner model

Assuming that the horizontal ( $x$ -direction) motion and the vertical ( $y$ -direction) motion are decoupled, the mechanical behavior of the scanner in the  $x$ -( $y$ )-directions can be modelled fairly accurately by two independent linear differential equations. Specifically, as shown in [5], a second-order model adequately captures the dynamics of the microscanner. The frequency response of the model in the  $y$ -direction has a resonance frequency of 138.1 Hz and a quality factor of approximately 13. However, such a model does not capture the cross-coupling between the axes. Figure 1 shows the cross-coupling on the  $y$ -axis due to  $x$ -motion for various offsets in the  $y$ -direction. As shown in this figure, the cross-coupling is nonlinear and position-dependent. For simulation purposes, a simplified model of the cross-coupling is used. This model is a quadratic fit of the cross-coupling as a function of the  $x$ -position, where the coefficients of the second-order equation change depending on the  $y$ -position. As shown in Fig. 1 there is a very good match between the measured and the simulated cross-coupling. Note that for the control design, the cross-coupling is treated as a disturbance signal that has to be rejected by the control.

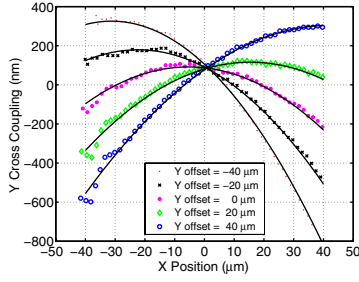


Fig. 1. Cross-coupling between the  $x$ - and  $y$ -axes. Marks represent the measured data; lines correspond to the quadratic fit.

### B. Thermal position sensors

The thermal sensors do not introduce any additional dynamics in the frequency region of interest, and can therefore be modelled as constant gains. Positioning accuracy is related to the intrinsic noise characteristics of the sensors. The standard deviation of the sensor noise has been measured to be approx. 2 nm over 5 kHz bandwidth. Although the accuracy of the sensor is reasonably good, there is a significant low-frequency component as can be seen from the power spectral density of the sensor noise shown in Fig. 2. The thermal sensors operate over the entire travel range of the micro-scanner and hence are capable of providing global-position information.

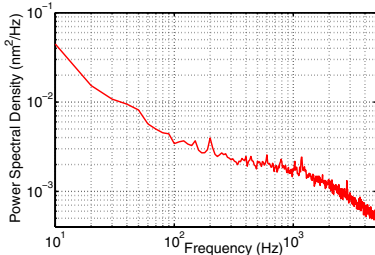


Fig. 2. Measured power spectral density of thermal-sensor noise.

### C. Medium-derived position-error signal (PES)

Besides the thermal position sensors, pre-written servo patterns on the medium can provide an alternate position signal. In fact, this signal measures the deviation of the cantilever tip from the track center during the read operation. The method to generate the medium-derived PES is based on the concept of mutually vertically displaced sequences of indentations (bursts), arranged in such a way as to produce two signals in quadrature, which can be combined to provide a robust PES [2]. Servo bursts labeled A and B are used to create the in-phase signal (I), and C and D the quadrature signal (Q). A, B, C and D bursts are written in four different dedicated storage fields, called servo fields. The cross-track distance between indentation centers of the same burst is equal to the track pitch (TP), whereas the distance between indentation centers in A and B (or C and D) bursts is TP/2. The distance between A and C centers is TP/4. The configuration of the servo bursts is illustrated in Fig. 3(a). The circles represent written indentations, and the track centerlines coincide with the centers of burst B.

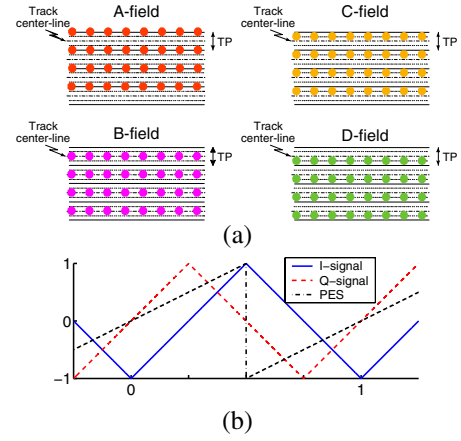


Fig. 3. (a) Servo-burst configuration; (b) ideal position-error signal.

To illustrate the principle of PES generation, let us assume that indentations in all bursts are spaced bit pitch (BP) units apart in the  $x$ -direction, and that sampling occurs exactly at the indentation centers. Referring to Fig. 3(a), let us further assume that the cantilevers move in the  $y$ -direction following a line crossing the centers of the indentations. For example, the cantilever of field A moves from the edge of the top indentation towards its center, then towards its bottom edge, then to a blank space, again to an indentation and so on. The amplitude of the readout signal is maximum at the indentation center and decreases with the distance from the center. The I-signal is synthesized as the difference  $\bar{B} - \bar{A}$ , where  $\bar{A}$  and  $\bar{B}$  correspond to the measured signal amplitudes in bursts A and B, respectively. The Q-signal is generated from the readback signals of bursts C and D as  $\bar{D} - \bar{C}$ . Note that the Q-signal exhibits zero crossings at points where the I-signal has local extrema, as shown in Fig. 3(b). A signal that has zero crossings at all track center locations, and linear range between  $-TP/2$  and  $TP/2$  can be generated by combining the two signals (I and Q) as shown in Fig. 3(a). The medium-derived PES provides positional information around each track centerline, and therefore has a maximum range of TP. Moreover, a reliable PES is obtained only after the probes have traversed a distance of one BP while scanning in the  $x$ -direction. Hence, PES is a discrete signal with the discrete time step equal to the time needed by the scanner to move a distance equal to BP in the  $x$ -direction.

## III. CONTROLLER DESIGN

### A. Two-sensor-based control configuration

As mentioned earlier, the objective is to design a joint controller that utilizes both the thermal sensor signal and the medium-derived PES. We assume that we operate around a track centerline so that medium-derived position information is available. The block diagram describing such a control architecture is shown in Fig. 4. In this configuration, G denotes the nominal model of the plant, that is, the microscanner model in the  $y$ -direction, and K represents the controller to be designed. The signal  $y$  describes the motion of the microscanner, whereas  $d$  and  $n$  denote the disturbance and

the noise signals, respectively. Signals  $y_{\text{PES}}$  and  $y_{\text{th}}$  denote the medium-derived PES and thermal sensor signal, respectively.

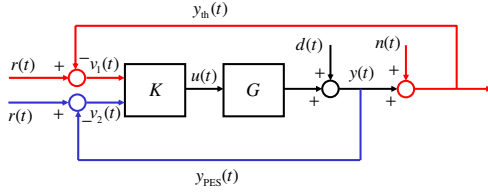


Fig. 4. Block diagram of two-sensor-based control configuration.

The objective is to design a controller such that it is able to take advantage of the unlimited range and high fidelity of the thermal sensor signal at high frequencies and of the low-frequency accuracy of PES signal. This problem can be formulated as a general control problem of a system that has two sensors with different noise characteristics at different frequencies. The objective is then to design a control structure that utilizes the best sensor in each frequency region.

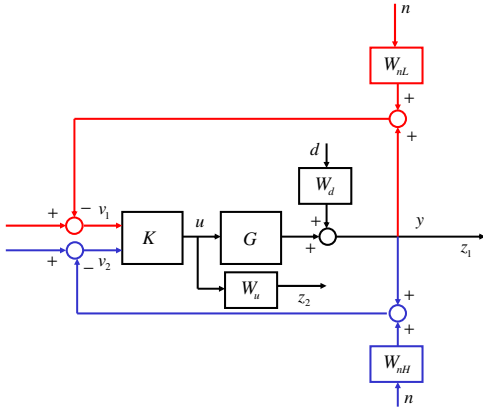


Fig. 5. Joint control formulation using weighting functions.

A formulation of this problem is shown in the block diagram of Fig. 5. Weighting functions are used to characterize the frequency content of the input signals, i.e., the disturbances and the noise sources, but also to impose constraints on the tracking error and the control effort. Specifically, the weight  $W_d$ , which describes the frequency content of the disturbances, has high gain at low frequencies because the cross-coupling that is the main disturbance source falls into this frequency region. The difference in noise characteristics of the two sensors is captured by the two weights  $W_{nL}$  and  $W_{nH}$ . The transfer function  $W_{nL}$  has low-pass filter characteristics that forces the signal  $v_1$  to be the preferred signal at high frequencies. On the other hand, the transfer function  $W_{nH}$  exhibits high-pass filter characteristics that make the signal  $v_2$  the preferred one at low frequencies. For the system under consideration,  $v_1$  can model the thermal sensor signal that has a significant low-frequency component. Finally, the medium-derived PES can be thought of as a second sensor with a fictitious high-frequency noise, as the requirement is to prefer the thermal sensor signal at higher frequencies. The weight  $W_u$  is used to impose constraints on the control signal.

This problem can be cast as an  $H_\infty$  optimization problem using the general control configuration [6], [7]. Using this

configuration, the exogenous input is  $\mathbf{w} = \begin{bmatrix} d \\ n \end{bmatrix}$ . Similarly, the error signal is  $\mathbf{z} = \begin{bmatrix} z_1 \\ z_2 \end{bmatrix}$ , where  $z_1 = y$  and  $z_2 = W_u u$ . The system can then be described by

$$\begin{bmatrix} \mathbf{z} \\ \mathbf{v} \end{bmatrix} = P \begin{bmatrix} \mathbf{w} \\ u \end{bmatrix} = \begin{bmatrix} P_{11} & P_{12} \\ P_{21} & P_{22} \end{bmatrix} \begin{bmatrix} \mathbf{w} \\ u \end{bmatrix}, \quad (1)$$

$$u = K\mathbf{v},$$

where  $\mathbf{v} = \begin{bmatrix} v_1 \\ v_2 \end{bmatrix}$  is the input to the controller and the elements of the generalized plant  $P$  are given by

$$P_{11} = \begin{bmatrix} W_d & 0 \\ 0 & 0 \end{bmatrix}, P_{12} = \begin{bmatrix} G \\ W_u \end{bmatrix}, \quad (2)$$

$$P_{21} = \begin{bmatrix} -W_d & -W_{nL} \\ -W_d & -W_{nH} \end{bmatrix}, P_{22} = \begin{bmatrix} -G \\ -G \end{bmatrix},$$

and the controller to be designed has the structure  $K = \begin{bmatrix} K_1 & K_2 \end{bmatrix}$ . The linear fractional transformation  $F_l(P, K)$ , defined as  $\mathbf{z} = F_l(P, K)\mathbf{w}$  is given by

$$F_l(P, K) = \begin{bmatrix} \frac{W_d}{1+GK_1+GK_2} & \frac{-GK_1W_{nL}-GK_2W_{nH}}{1+GK_1+GK_2} \\ \frac{-W_uW_d(K_1+K_2)}{1+GK_1+GK_2} & \frac{-W_u(K_1W_{nL}+K_2W_{nH})}{1+GK_1+GK_2} \end{bmatrix}, \quad (3)$$

The objective of the standard  $H_\infty$  optimal control is to find a stabilizing controller  $K$  that minimizes the following, [7]:

$$\|F_l(P, K)\|_\infty = \max_{\omega} \bar{\sigma}(F_l(P, K)(j\omega)). \quad (4)$$

In practice, we solve the  $H_\infty$  sub-optimal control problem where we find a stabilizing controller that provides an upper bound  $\gamma$  to the  $H_\infty$  norm [7]:

$$\|F_l(P, K)\|_\infty < \gamma. \quad (5)$$

Note that the performance objectives are met if  $\gamma \leq 1$ .

Let  $S_{\text{dis}}$  and  $T_{\text{noise}}$  be the closed-loop transfer functions from disturbance  $d$  to output  $y$  and from noise  $n$  to output  $y$ , respectively. The equations that describe these transfer functions for the system shown in Fig. 4 are given by

$$S_{\text{dis}} = \frac{1}{1+GK_1+GK_2}, T_{\text{noise}} = \frac{-GK_1}{1+GK_1+GK_2}. \quad (6)$$

From (3) and (5) it is clear that the choice of  $W_d$  yields an upper bound on  $S_{\text{dis}}$  and therefore captures the disturbance-rejection requirements. Also, the choice of  $W_{nL}$  and  $W_{nH}$  determines the distribution of the gain of  $K_1$  and  $K_2$  as a function of frequency. This choice will eventually give the desired frequency response for  $T_{\text{noise}}$ .

Equation (7) gives the expressions for  $T_{\text{ref}}$ , the transfer function from the reference to the output, and  $S_{\text{ref}}$  the transfer function from references  $r$  to the error  $r - y$ . Specifically,

$$T_{\text{ref}} = \frac{GK_1+GK_2}{1+GK_1+GK_2}, S_{\text{ref}} = \frac{1}{1+GK_1+GK_2}. \quad (7)$$

From these equations, we observe that  $S_{\text{ref}}$  is equal to  $S_{\text{dis}}$  as in a one-degree-of-freedom control architecture. Therefore, the constraints imposed on  $S_{\text{dis}}$  are also valid for  $S_{\text{ref}}$ . As our main disturbance is the cross-coupling that has similar frequency content as the reference signal, there is no need for additional constraints.

## B. Joint controller design based on thermal-sensor signal and medium-derived PES

A joint controller based on the thermal-sensor signal and medium-derived PES was designed using the scheme described above. The microscanner and thermal-position-sensor characteristics along with the performance requirements were translated into appropriate weighting functions. The weighting function  $W_d$  was chosen as  $W_d = \frac{s+12.57}{s+12.57}$ . This choice was made to yield rejection capabilities at low frequencies and to achieve a closed-loop bandwidth of 200 Hz. The frequency region in which the thermal-sensor information is not reliable can be specified by the weighting function  $W_{nL}$ , which was chosen as  $W_{nL} = \frac{0.0001s+12.57}{s+0.1257}$ . As the thermal-sensor signal has a low-frequency component,  $W_{nL}$  is designed to have high gains at very low frequencies up to 2 Hz and low gains at high frequencies. The weighting function  $W_{nH}$  is given by  $W_{nH} = \frac{s+0.03142}{s+314.2}$  and was chosen such that the joint controller relies more strongly on the thermal sensor than on the PES for frequencies higher than 50 Hz. The weighting function,  $W_u$ , was chosen to limit the control effort such that the given power dissipation constraints are satisfied.

A 5<sup>th</sup>-order controller with two inputs and one output is obtained from the design based on the  $H_\infty$  optimal control. The joint controller has a transfer function  $K_1$  from the thermal-sensor error signal to the output and a transfer function  $K_2$  from the PES to the output. Figure 6 shows the frequency response of the two elements  $K_1$  and  $K_2$  of the joint controller. The transfer function  $K_1$  that uses as input the thermal-sensor signal has smaller gain at low frequencies than  $K_2$ , which uses the PES signal as input. At higher frequencies, the gain of  $K_1$  is higher than that of  $K_2$ . The shape of the resulting transfer functions is in agreement with the design specifications. The point at which the two transfer functions intercept, which specifies where each of the two inputs to the controller will predominate, can be changed by appropriately modifying the weights  $W_{nL}$  and  $W_{nH}$ .

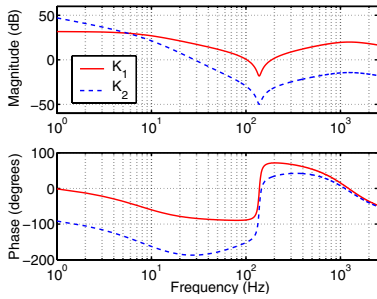


Fig. 6. Frequency response of the joint controller elements.

Figure 7 shows the frequency response of the closed-loop transfer functions  $T_{ref}$ ,  $S_{dis}$ , and  $T_{noise}$ . The low gain of  $S_{dis}$  at low frequencies shows that the closed-loop system suffices to reject disturbances up to approximately 130 Hz. As  $S_{ref}$  is equal to  $S_{dis}$ , the bandwidth of the closed-loop system, that is, the frequency where the magnitude of  $S_{ref}$  first crosses  $-3$  dB from below, is 130 Hz. The low gain of  $T_{noise}$  at low frequencies is another good indication that the design meets the specifications as any noise input at these frequencies will not affect the scanner motion.

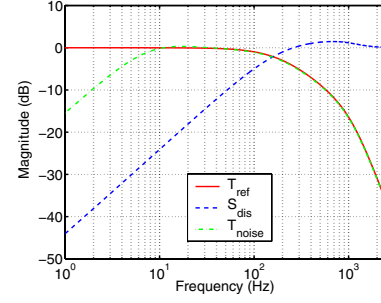


Fig. 7. Frequency response of closed-loop transfer functions.

## IV. EXPERIMENTAL RESULTS

The proposed control architecture was implemented and demonstrated in an experimental setup that includes the microscanner and the cantilever array chip. The performance of the joint control architecture is compared with that of the thermal-sensor-based control described in [5].

### A. Medium-derived PES generation

For the purpose of generating medium-derived PES information, A, B, C and D bursts were written on the polymer medium using four cantilevers on their respective storage fields. The track pitch and bit pitch were set to 60 nm. Accordingly, the cross-track distance between the A(C) and B(D) bursts equals 30 nm. To depict the servo pattern, a scan of 30 lines was performed stepping by 5 nm in the  $y$ -direction. Four samples of the readback signal per written indentation were used to correlate with a pulse shape representing a typical indentation and to measure the indentation depth. The average indentation depth obtained over each line from the A, B, C and D servo fields is shown in Fig. 8.

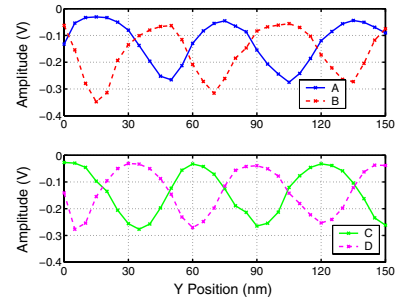


Fig. 8. A, B, C and D indentation profiles.

The resulting in-phase and quadrature signals are shown in Fig. 9. We observe that the zero crossings of the quadrature signal align with the positions of the maximum signal of either A or B bursts, with the zero crossing of positive slope corresponding to B bursts. In the implementation of the joint control architecture, only the quadrature signal is used as input to the controller with the track-center line coinciding with the B bursts. Note that there is no loss of generality in the use of the quadrature signal alone. It solely results in a further reduction in the range of the PES.

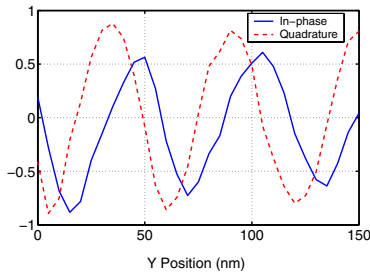


Fig. 9. In-phase and quadrature signals.

### B. Thermal-sensor-based control

A servomechanism for the microscanner that uses the position information from the thermal sensors only was presented in [5]. Specifically, two decoupled feedback loops for the  $x$ - and  $y$ -directions were designed based on the linear quadratic Gaussian approach. Using this control scheme, we performed a simultaneous read operation using the four servo levers while scanning along the  $x$ -direction with a linear velocity of  $0.3 \text{ nm}/\mu\text{s}$ . The reference signal on the  $y$ -axis is kept constant to a position close to the track centerline of servo lever B. Figure 10 shows the readback signal from the four servo fields for 50 line scans.

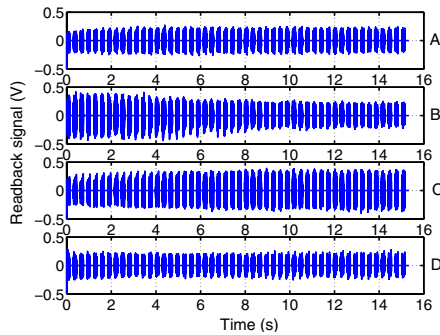


Fig. 10. Thermal-sensor-based control: Readback signal from the four cantilevers.

We observe that although the  $y$ -axis reference is kept constant, the magnitude of the readback signal from servo field B is higher in the first few scans but decreases in the later scans. This means that the tip moves from a position close to the center of the indentations towards the edges and finally completely out of the indentations. In contrast, the magnitude of the signal from servo field C is small in the first few scans, but increases to and stabilizes at a high value in the last scans. This can be better observed from the plot of the average magnitude of the indentation depth over each line scan shown in Fig. 11. This behavior can be explained by a possible drift on the thermal-sensor signal that would be erroneously used by the controller to correct the position of the scanner. As the distance between centers of bursts B and C is equal to  $TP/4$ , in our case  $15 \text{ nm}$ , an estimated value of the drift is between  $15$  and  $30 \text{ nm}$ .

Another way to measure the motion in the  $y$ -direction is to use the control effort supplied by the controller. Subtracting the control effort of the first scan from that of the subsequent scans yields a measure of the drift. This assumes that the

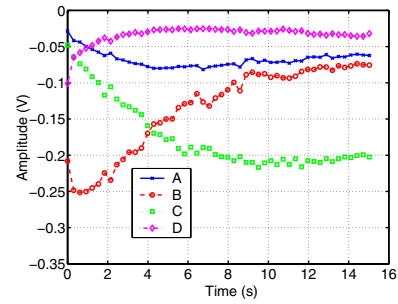


Fig. 11. Thermal-sensor-based control: A, B, C and D indentation profiles.

cross coupling remains constant between successive scans, which is valid as the motion in the  $x$ -axis remains the same for all scans and the  $y$ -reference is constant. Figure 12 shows the  $y$ -motion calculated from the control effort, which shows that the estimated drift is  $30 \text{ nm}$  at the end of 50 scans, in accordance with the previous result. In the same figure, the  $y$ -motion as measured from the thermal sensors appears constant, because the control loop has corrected for the drift. This experiment clearly shows the adverse effect of the low-frequency noise on the thermal position sensor.

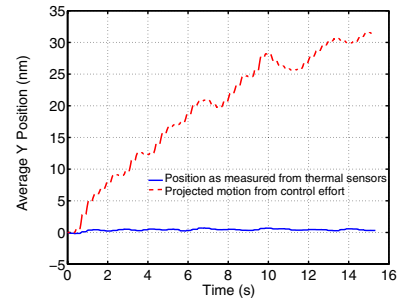


Fig. 12. Thermal-sensor-based control:  $y$ -sensor output and projected motion from the control effort.

### C. Joint control

The joint controller designed in the preceding section has been realized in a digital signal processor. No PES information is available during seek and in backward scan directions because no read operation is performed. Therefore, both sensors are active during the positive direction of the scan, and when no PES information is available, the PES signal is set to zero and control is based exclusively on the thermal sensors. As the controller is of the MISO type, there is no need to switch between different controllers when one of the sensor signals is not available.

Using the joint-control architecture we repeat the same experiment as described in the preceding section. Figure 13 shows the readback signal from the four servo fields for 50 scans. Clearly, the magnitude of the signal from servo field B remains high throughout the experiment. Figure 14 shows the average magnitude of the indentation depth over each line scan. This result shows that the position of the probes is such that the cantilever of servo field B is always on top of the center of the indentation bursts B and the other three cantilevers are outside of the indentation bursts A, C and

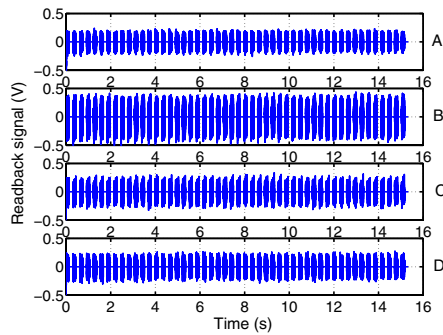


Fig. 13. Joint control: Readback signal from the four cantilevers.

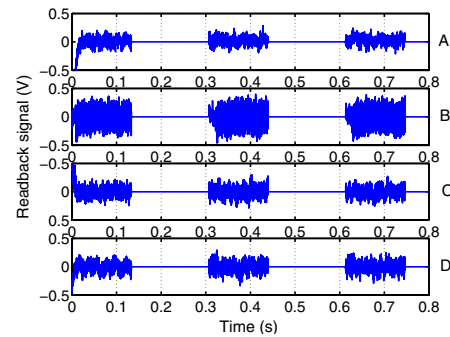


Fig. 16. Joint control: Readback signal from the four cantilevers.

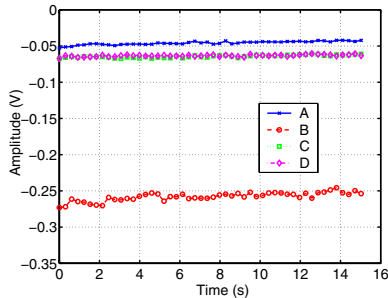


Fig. 14. Joint control: A, B, C and D indentation profiles.

D. As the centers of indentation B were defined as the track centerlines, the tracking requirement is satisfied and tracking is immune to the low-frequency noise due to the thermal position sensors.

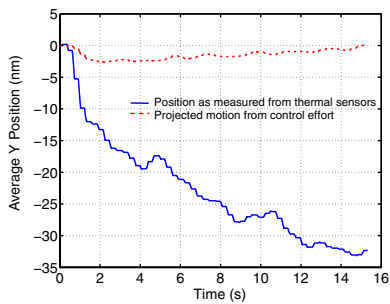


Fig. 15. Joint control: y-sensor output and projected motion from the control effort.

The result can be verified again from the y-motion projected from the control effort as shown in Fig. 15. As can be seen, the y-motion remains constant although the signal from the thermal sensors indicates a motion of approx. 30 nm. Therefore, with this scheme thermal-sensor drift will not affect scanner motion. Moreover, while the control is based on both sensors, the low frequency fidelity of the PES signal could be exploited to make periodic corrections for the drift on the thermal-sensor signal.

Another experiment that verifies the robustness of the proposed architecture is that of navigation through the tracks. The readback signal from the four levers while navigating through three different tracks is shown in Fig. 16. Again we observe that the signal from cantilever B is the highest throughout the experiment. This indicates that accurate probe

positioning and subsequent track following, as required for reliable data storage, can be achieved using the proposed joint controller architecture.

## V. CONCLUSIONS

In probe-storage applications the probes have to be positioned over the storage medium with nanoscale accuracy. A global-positioning sensor can provide the required accuracy but has significant low-frequency noise. On the other hand, a medium-derived position-error signal does not suffer from low-frequency noise but has limited range. A novel control architecture is presented that utilizes both the global-positioning sensor and the medium-derived position signal. A frequency-separated control method is developed that uses the best measurement in different frequency regions.

## VI. ACKNOWLEDGMENTS

We thank our colleagues of the Probe Storage group at IBM Zurich Research Laboratory. Special thanks go to M. Despont, U. Drechsler, D. Jubin, M. Lantz and H. Rothuizen for the design and fabrication of the MEMS parts, P. Bächtold for the design of the electronics, and G. Cherubini for useful discussions. We also thank the group of T. Antonakopoulos at the University of Patras, Greece, for their contributions to this work.

## REFERENCES

- [1] P. Vettiger, G. Cross, M. Despont, U. Drechsler, U. Dürig, B. Gotsmann, W. Häberle, M.A. Lantz, H.E. Rothuizen, R. Stutz, and G.K. Binnig. The “millipede”-nanotechnology entering data storage. *IEEE Trans. Nanotechnology*, 1:39–55, 2002.
- [2] E. Eleftheriou, T. Antonakopoulos, G. K. Binnig, G. Cherubini, M. Despont, A. Dholakia, U. Durig, M. A. Lantz, H. Pozidis, H. E. Rothuizen, and P. Vettiger. Millipede-a MEMS based scanning-probe data storage system. *IEEE Transactions on Magnetics*, 39(2):pp. 938–945, 2003.
- [3] A. Pantazi, M. A. Lantz, G. Cherubini, H. Pozidis, and E. Eleftheriou. A servomechanism for a micro-electro-mechanical-system-based scanning-probe data storage device. *Nanotechnology*, 15:612–621, August 2004.
- [4] M. A. Lantz, G. K. Binnig, M. Despont, and U. Drechsler. A micro-mechanical thermal displacement sensor with nanometer resolution. *Nanotechnology*, 16:1089–1094, May 2005.
- [5] A. Sebastian, A. Pantazi, G. Cherubini, E. Eleftheriou, M. Lantz, and H. Pozidis. Nanopositioning for probe storage. In *Proceedings of the American Control Conference, Portland, Oregon*, pages 4181–4186, June 2005.
- [6] K. Zhou, J. C. Doyle, and K. Glover. *Robust and Optimal Control*. Prentice Hall, Englewood Cliffs, 1995.
- [7] S. Skogestad and I. Postlethwaite. *Multivariable Feedback Control, Analysis and Design*. John Wiley and Sons, New York, 1997.